# Dalton Transactions



PAPER

View Article Online
View Journal | View Issue



**Cite this:** *Dalton Trans.*, 2025, **54**, 14710

# Electrocatalytic urea synthesis from NO and CO<sub>2</sub> on In<sub>1</sub>Pd single atom alloys

Tingting Wu, \*a Zihan Tian, a Ziyang Zhang, Ye Tian and Ke Chu \*b

Electrocatalytic urea synthesis from  $CO_2/NO$  co-electrolysis (EUCN) has emerged as a promising strategy for sustainable urea production, while simultaneously mitigating greenhouse gas emissions and NO pollutants. Herein, we have developed single-atom  $In_1$  alloyed Pd ( $In_1Pd$ ) as a high-performance EUCN catalyst, delivering a remarkable  $FE_{urea}$  of 45.9% and a urea yield rate of 55.2 mmol  $h^{-1}$   $g^{-1}$  in a membrane electrode assembly electrolyzer. The combination of *in situ* spectroscopic measurements and theoretical calculations reveals the synergy of  $In_1$  and Pd, which enables the co-activation of  $CO_2/NO$  and their C-N coupling while hampering the competing reactions, leading to greatly enhanced EUCN activity and selectivity.

Received 22nd August 2025, Accepted 5th September 2025 DOI: 10.1039/d5dt02018b

rsc.li/dalton

Urea is a vital nitrogen fertilizer that is widely used in global agriculture.1-3 Currently, the Bosch-Meiser process serves as the primary industrial route for urea synthesis, accounting for over 2% of global energy consumption and generating substantial CO<sub>2</sub> emissions. 4-8 Electrocatalytic urea synthesis from co-reduction of CO2 and NO (EUCN) has emerged as a promising strategy for sustainable urea production, while simultaneously mitigating greenhouse gas emissions and NO pollutants.9 However, the EUCN process involves a complex multistep reaction pathway requiring the activation of inert CO2 and NO molecules and enhanced C-N coupling kinetics, posing significant challenges for catalyst design.<sup>10</sup> Current catalysts still suffer from low urea faradaic efficiency (FEurea) and poor selectivity due possibly to the competitive side reactions (i.e., the hydrogen evolution reaction (HER)) and independent reduction pathways.9 Therefore, the development of high-performance catalysts with high activity, selectivity and durability is crucial to advance the practical application of EUCN.

Single-atom alloys (SAAs), which combine the merits of single-atom catalysts and alloy catalysts, have garnered significant attention in various electrocatalytic reactions involving both carbon and nitrogen cycles,  $^{11-13}$  thus demonstrating their considerable potential for electrocatalytic urea synthesis from CO<sub>2</sub>/NO co-electrolysis (EUCN). Among them, Pd-based materials have shown particular efficacy attributed to their unfilled d-electron orbitals ( $^{4}$ d $^{10}$ ) that facilitate optimized adsorption/desorption behavior of key intermediates.  $^{14-16}$  Nevertheless, Pd-based catalysts often suffer from insufficient

co-activation capability toward both nitrogen and carbon sources. Additionally, Pd exhibits a strong tendency for H adsorption, <sup>17</sup> which competes with the C–N coupling reaction and diminishes both EUCN activity and selectivity for urea synthesis. Notably, these limitations may be effectively mitigated by incorporating p-block metals such as indium (In). By virtue of its partially occupied p-orbitals, In can intrinsically hinder H binding, <sup>18</sup> while promoting CO<sub>2</sub> reduction to generate and stabilize C-intermediates beneficial for coupling with N-intermediates towards urea generation. <sup>19–21</sup> Motivated by these insights, we propose that single-atom In alloyed with Pd (In<sub>1</sub>Pd) may serve as a highly promising catalyst, enabling enhanced activity and selectivity for efficient EUCN.

In this study, we developed  $In_1Pd$  as a highly active and selective EUCN catalyst for urea electrosynthesis. Notably, the  $In_1Pd$  catalyst exhibits exceptional performance in a membrane electrode assembly (MEA) electrolyzer, delivering a remarkable  $FE_{urea}$  of 45.9% and a urea yield rate of 55.2 mmol  $h^{-1}$   $g^{-1}$  at -0.7 V. The catalytic EUCN mechanism of the  $In_1Pd$  catalyst is further elucidated through combined *in situ* spectroscopic measurements and theoretical calculations, revealing that the enhanced EUCN efficiency of  $In_1Pd$  stems from the synergistic effect of  $In_1$  and Pd, which promotes the co-activation of  $CO_2$  and Pd0 to Pd1 and Pd2 and their Pd3 coupling.

In<sub>1</sub>Pd was synthesized *via* a one-pot wet chemistry method. The XRD patterns (Fig. 1a) reveal that In<sub>1</sub>Pd retains the crystalline structure of pristine Pd (JCPDS No. 65-2867), suggesting that In<sub>1</sub> incorporation does not change the crystalline phase of pristine Pd. The TEM image (Fig. 1b) shows that In<sub>1</sub>Pd exhibits a typical graphene-like morphology. Elemental mapping images of In<sub>1</sub>Pd (Fig. 1c) illustrate a uniform distribution of In<sub>1</sub> atoms on Pd. The coordination structure and electronic characteristics of In<sub>1</sub>Pd are systematically characterized *via* 

<sup>&</sup>lt;sup>a</sup>College of Science, Hebei North University, Zhangjiakou 075000, Hebei, China. E-mail: 1329271270@aa.com

bSchool of Materials Science and Engineering, Lanzhou Jiaotong University, Lanzhou 730070, China. E-mail: chuk630@mail.lzjtu.cn

**Dalton Transactions** 

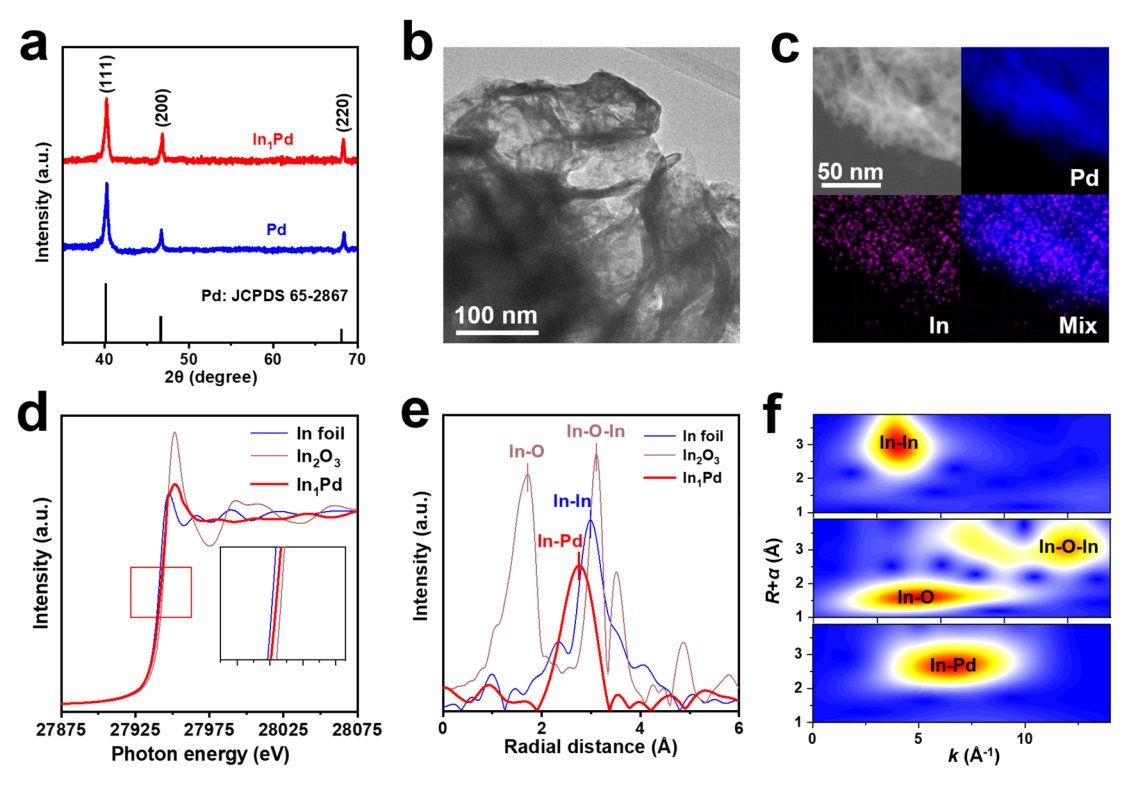


Fig. 1 Characterization of In<sub>1</sub>Pd: (a) XRD patterns, (b) TEM image, (c) elemental mapping images, (d) In K-edge XANES, (e) EXAFS spectra and (f) WT analyses of In<sub>1</sub>Pd and reference samples.

X-ray absorption spectroscopy. The XANES analysis at the In K-edge (Fig. 1d) reveals that the absorption edge of In₁Pd lies between In foil and In<sub>2</sub>O<sub>3</sub> reference samples, indicating an In oxidation state between 0 and +3, which arises from electron transfer from In<sub>1</sub> to Pd due to the lower electronegativity of In (1.78) relative to Pd (2.20). The EXAFS spectra (Fig. 1e) show that In<sub>1</sub>Pd exhibits a prominent In-Pd coordination peak at 2.75 Å, with no observable In-In or In-Pd coordination bonds, confirming the atomic dispersion of In on the Pd substrate. 22-24 The corresponding wavelet transform (WT) analysis (Fig. 1f) displays a single In-Pd coordination peak at  $6.5 \text{ Å}^{-1}$ , further verifying the monoatomic In dispersion within the Pd matrix.

The electronic structure of In<sub>1</sub>Pd is systematically investigated using DFT calculations. Electron density difference analysis (Fig. S1a) reveals a distinct electron transfer from In<sub>1</sub> to Pd, in line with the XANES result (Fig. 1d). This interfacial In<sub>1</sub>-Pd electron interaction guarantees the robust bonding between In<sub>1</sub> and the Pd substrate, which endows In<sub>1</sub>Pd with exceptional structural stability. The corresponding PDOS analysis (Fig. S1b) presents favorable orbital overlapping between the 5p orbital of In<sub>1</sub> and the 4d orbital of Pd, offering a theoretical foundation for the efficient charge transfer and robust structural stability.<sup>25</sup> Additionally, ab initio molecular dynamics (AIMD) simulation results (Fig. S2) indicate that In₁Pd maintains stable energy and temperature profiles throughout the simulation, further validating its excellent thermal stability. 26-30

The EUCN performance of In<sub>1</sub>Pd is assessed in a MEA cell containing 0.1 M KHCO<sub>3</sub> catholyte saturated with humidified NO and CO2. Gas and liquid products are quantified by gas chromatography and colorimetry, respectively (Fig. S3). LSV curves (Fig. 2a) show a relatively low current density of In<sub>1</sub>Pd in sole CO2-saturated electrolyte. Strikingly, the current density is significantly enhanced in the presence of both NO and CO<sub>2</sub>, suggesting the high catalytic EUCN activity of In<sub>1</sub>Pd toward urea synthesis. The EUCN performance of In₁Pd is quantitatively evaluated after 1 h of electrolysis. Remarkably, In<sub>1</sub>Pd achieves the highest FE<sub>urea</sub> of 45.9% at -0.7 V, with a corresponding urea yield rate of 55.2 mmol h<sup>-1</sup> g<sup>-1</sup> (Fig. 2b), surpassing most recently reported catalysts for urea electrosynthesis (Fig. S4 and Table S1). Control experiments are conducted to validate the nitrogen and carbon sources (Fig. S5). No urea formation is observed under conditions lacking NO or CO2, or at the open-circuit potential (OCP), effectively ruling out the possibility of system contamination as C/N sources of urea. Further <sup>13</sup>C and <sup>15</sup>N isotope tracing via nuclear magnetic resonance (NMR) spectroscopy, using \$^{13}CO\_2\$ (Fig. 2c) and \$^{15}NO\$ (Fig. 2d) as tracers, reveals the characteristic signals of <sup>13</sup>CO (NH<sub>2</sub>)<sub>2</sub> and CO(<sup>15</sup>NH<sub>2</sub>)<sub>2</sub>, respectively, further confirming that the synthesized urea originates exclusively from the EUNC process catalyzed by In<sub>1</sub>Pd.

Paper

b а C NO + 13CO2 Urea yield rates (mmol h<sup>-1</sup> g<sup>-1</sup> Currrent density (mA cm<sup>-2</sup>) -10 50 Intensity (a.u.) 40 Standard 13CO(NH<sub>2</sub>) 30 -30 NO+CO. 20 -0.4 -0.2 180 170 160 150 Poential (V vs. RHE) Potential (V vs. RHE) Chemical shift (ppm) d (mmol h<sup>-1</sup> g<sup>-1</sup>) CO2 + 15NO Intensity (a.u.) Jrea yield rates Standard CO(15NH<sub>2</sub>)<sub>2</sub> **Urea yield** 

Fig. 2 (a) LSV curves of  $In_1Pd$  under different conditions. (b) Urea yield rates and  $FE_{urea}$  of  $In_1Pd$  at various potentials. (c)  $^{13}C$  NMR spectra of the  $^{13}CO(NH_2)_2$  standard sample and those fed by  $^{13}CO_2$  after electrolysis at -0.7 V. (d)  $^{1}H$  NMR spectra of the  $CO(^{15}NH_2)_2$  standard sample and those electrolyzed in  $^{15}NO$  electrolyte at -0.7 V. (e) Urea yield rates and  $FE_{urea}$  during eight cycling tests at -0.7 V. (f) Comparison of urea yield rates and  $FE_{urea}$  between pristine Pd and  $In_1Pd$  at -0.7 V.

Cycle number

The selectivity of  $\rm In_1Pd$  toward ECNU is evaluated by quantifying the FEs of other byproducts (CO,  $\rm H_2$  and  $\rm NH_4^+$ ). At the optimal applied potential of -0.7 V,  $\rm FE_{urea}$  remains significantly higher than the FEs of all byproducts (Fig. S6), confirming the exceptional ECNU selectivity of  $\rm In_1Pd$  for urea synthesis. For stability evaluation, we conducted an eight-cycle test, which shows that both urea yield rate and  $\rm FE_{urea}$  exhibit minimal fluctuations (Fig. 2e), confirming the excellent catalysis durability of  $\rm In_1Pd$ .  $^{30-32}$  Comparative analysis shows that the pristine Pd catalyst (Fig. 2f) exhibits a much inferior ECNU performance relative to  $\rm In_1Pd$ , highlighting the critical synergistic interaction between  $\rm In_1$  and the Pd substrate in boosting the ECNU activity.

5.2 5.3 5.4 5.5 5.6 5.7

Chemical shift (ppm)

To elucidate the fundamental understanding of the significantly improved EUCN performance of  $In_1Pd$ , we employed *in situ* FTIR and online differential electrochemical mass spectrometry (DEMS) to identify the reaction intermediates. First, *in situ* FTIR measurements are conducted on  $In_1Pd$  over the potential range from the OCP to -0.7 V. As shown in Fig. 3a–c, the characteristic peak at 1396 cm<sup>-1</sup> is assigned to the symmetric stretching vibration of the \*COOH intermediate, while the C=O stretching peak at 2017 cm<sup>-1</sup> corresponds to the generated \*CO intermediate<sup>33</sup> (Fig. 3b). Notably, additional peaks observed at 1695 cm<sup>-1</sup> and 1433 cm<sup>-1</sup> are attributed to \*CONH<sub>2</sub> intermediates and C-N bonds, <sup>34–36</sup> respectively (Fig. 3c), indicating that EUCN proceeds via \*NH<sub>2</sub> + \*CO  $\rightarrow$  \*NH<sub>2</sub>CO. Meanwhile, the enhanced peak intensity of urea (1610/1195 cm<sup>-1</sup>) with increasing potentials indicates that the

generated \*NH<sub>2</sub>CO intermediates are readily converted into urea.<sup>35</sup> In addition, online DEMS measurements (Fig. 3d) show the prominent m/z signals corresponding to key intermediates and products, including \*CONH<sub>2</sub> (m/z = 44), \*CO (NH<sub>2</sub>)<sub>2</sub> (m/z = 60), \*NO (m/z = 30), \*NH<sub>2</sub> (m/z = 16), \*CO (m/z = 28) and \*COOH (m/z = 45). These DEMS results are in line with *in situ* FTIR data, collectively providing compelling evidence that In<sub>1</sub>Pd facilitates the efficient co-reduction of CO<sub>2</sub> and NO to urea through a sequential relay catalysis mechanism (Fig. S7), where In<sub>1</sub>Pd first promotes the co-activation of CO<sub>2</sub> and NO, forming critical \*CO and \*NH<sub>2</sub> intermediates. These \*CO/\*NH<sub>2</sub> intermediates then undergo C-N coupling to generate \*CONH<sub>2</sub>, which is ultimately converted into urea.

DFT calculations are utilized to unravel the atomic-level EUCN mechanism of  $In_1Pd$ . Given that the adsorption and activation of  $NO/CO_2$  represent the initial step of the catalytic EUCN process, our analysis first focused on  $NO/CO_2$  adsorption behaviors on both  $In_1$  and Pd sites of  $In_1Pd$ . As illustrated in Fig. S8, the adsorption free energy calculations reveal that  $In_1$  sites are more favorable for  $CO_2$  adsorption (-0.26 eV), while Pd sites are more favorable for NO adsorption (-0.48 eV), suggesting that during the EUCN process,  $In_1$  sites primarily facilitate  $CO_2$  reduction while Pd sites dominate NO reduction.

We then constructed the free energy diagram for the conversion of CO<sub>2</sub> to \*CO on In<sub>1</sub> sites (Fig. 4a), with the corresponding intermediate configurations shown in Fig. S9. Calculation results reveal that the rate-determining step (RDS)

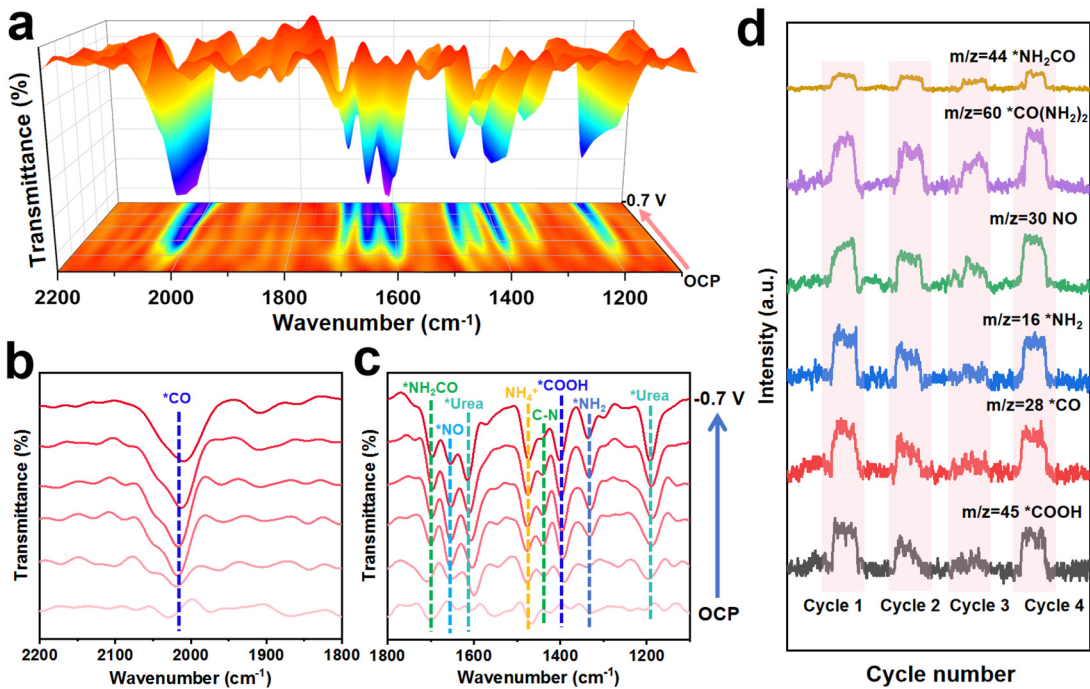


Fig. 3 (a-c) In situ FTIR spectra of  $In_1Pd$  during the EUNC electrolysis at different potentials from the OCP to -0.7 V. (d) Online DEMS spectra of  $In_1Pd$  at -0.7 V.

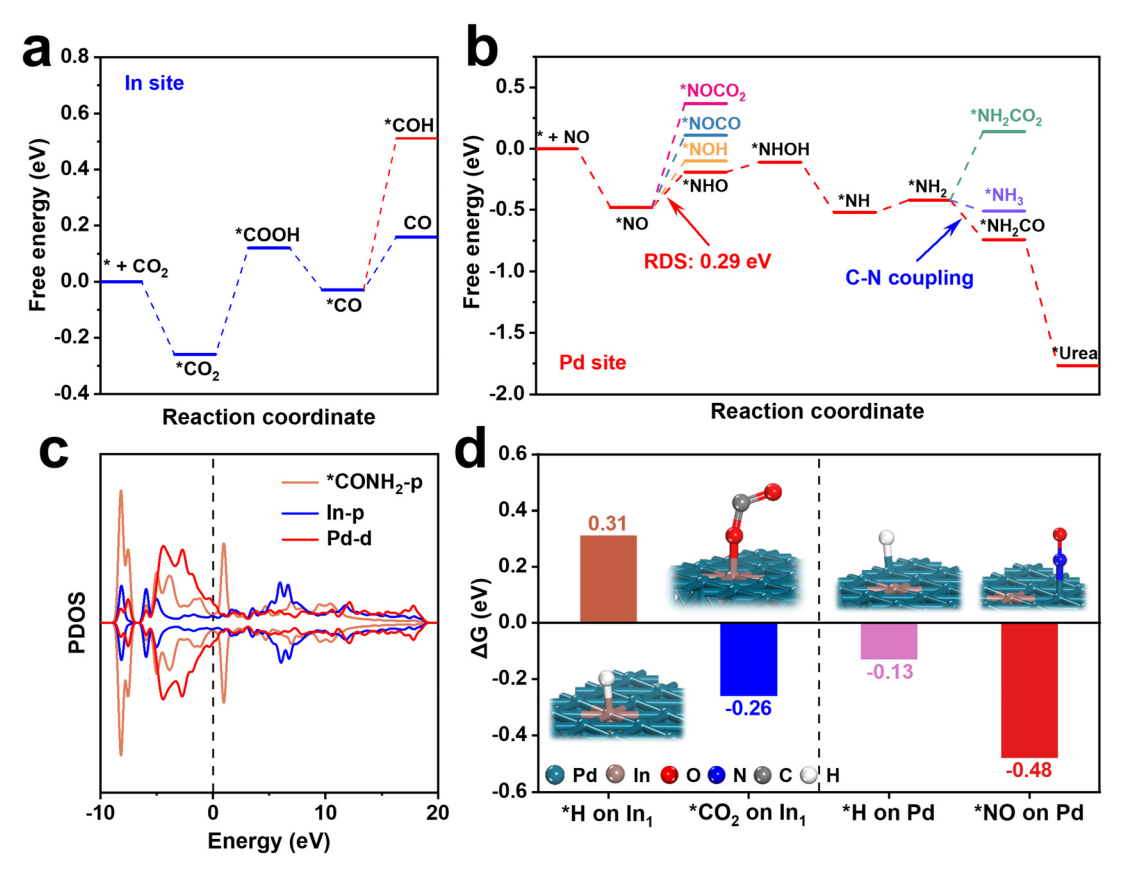


Fig. 4 (a) Free energy diagram of the  $CO_2 \rightarrow CO$  pathway on  $In_1$  sites. (b) Free energy diagram of the entire EUNC pathway on Pd sites and possible competing side reactions. (c) PDOS profile of \*CONH<sub>2</sub> on  $In_1$ Pd. (d) Adsorption free energies of \*H/\*CO<sub>2</sub> on  $In_1$  sites and \*H/\*NO on Pd sites.

**Paper Dalton Transactions** 

for  $CO_2 \rightarrow *CO$  reduction is the first  $CO_2$  hydrogenation (\* $CO_2$ ) + \*H → \*COOH), with an energy barrier of 0.38 eV. Notably, the \*CO desorption energy barrier on In<sub>1</sub> sites is significantly lower (0.19 eV) than that required for further hydrogenation (\*CO + \*H  $\rightarrow$  \*COH, 0.54 eV), indicating that \*CO generated on In<sub>1</sub> sites is more inclined to desorb and spontaneously migrate closer to Pd sites and participate in the C-N coupling reaction.

Subsequently, we constructed the free energy diagram for the entire EUCN process on Pd sites, with the corresponding intermediate configurations shown in Fig. S10. As illustrated in Fig. 4b, the RDS of this pathway is also the initial NO hydrogenation (\*NO + \*H  $\rightarrow$  \*NHO, 0.29 eV). Further analysis of the energy barriers for the competing reactions, such as \*NO + \*CO  $\rightarrow$  \*NOCO and \*NO + \*CO<sub>2</sub>  $\rightarrow$  \*NOCO<sub>2</sub>, reveals that compared to direct C-N coupling with \*CO or \*CO2, \*NO tends to undergo hydrogenation reduction via the NHO pathway. Significantly, after stepwise \*NOH reduction to \*NH2, the generated \*NH2 intermediate is more likely to undergo C-N coupling with \*CO to form \*NH2CO relative to other competing reactions (\*NH<sub>2</sub> + H  $\rightarrow$  \*NH<sub>3</sub>, \*NH<sub>2</sub> + CO<sub>2</sub>  $\rightarrow$  \*NH<sub>2</sub>CO<sub>2</sub>). The generated \*NH2CO can be spontaneously converted into urea. These findings correlate closely with the above in situ FTIR and DEMS results (Fig. 3).

For the critical \*NH2CO intermediate on both pristine Pd and In<sub>1</sub>Pd surfaces (Fig. S11), the charge density difference map displays that In<sub>1</sub>Pd provides more electrons to \*NH<sub>2</sub>CO than pristine Pd does, suggesting the significantly enhanced \*NH<sub>2</sub>CO stabilization on In<sub>1</sub>Pd. Further PDOS analysis (Fig. 4c and Fig. S12) reveals that compared to pristine Pd, the overlap region of electron orbitals between In<sub>1</sub>Pd and \*NH<sub>2</sub>CO is much expanded, further verifying the stronger \*NH2CO activation capability of In<sub>1</sub>Pd. These results indicate that the introduced In<sub>1</sub> not only promotes the reduction of CO<sub>2</sub> to \*CO but also modulates the electronic structure of the Pd substrate and enhances \*NH2CO stabilization and activation towards urea conversion. Given the HER as the major competing reaction for the EUCN, we examined the adsorption characteristics of \*H on In<sub>1</sub>Pd. Fig. 4d shows that In<sub>1</sub> sites are more favorable for adsorbing \*CO2 over \*H, while Pd sites exhibit a stronger tendency to adsorb \*NO over \*H. Molecular dynamics (MD) simulations (Fig. S13) further reveal a more pronounced enrichment effect of \*NO on the In<sub>1</sub>Pd surface, and the corresponding radial distribution function (RDF, Fig. S14) shows that the NO/In<sub>1</sub>Pd interaction is stronger than the H/In<sub>1</sub>Pd interaction. These results demonstrate that In<sub>1</sub>Pd can well hamper the competing HER towards the selective conversion of CO<sub>2</sub>/NO to urea.

In summary, In<sub>1</sub>Pd is demonstrated as a high-performance EUCN catalyst for urea electrosynthesis. Combined in situ spectroscopic measurements and theoretical calculations reveal that the enhanced EUCN performance of In<sub>1</sub>Pd stems from the synergy of In<sub>1</sub> and Pd, which enables the co-activation of CO<sub>2</sub>/NO and their C-N coupling, while hampering the competing reactions. Impressively, In<sub>1</sub>Pd exhibits an unprecedented urea synthesis performance with urea yield rate up to 55.2 mmol h<sup>-1</sup> g<sup>-1</sup> and FE<sub>urea</sub> of 45.9% in a MEA cell. This

work provides in-depth insights into the EUCN mechanism and opens up a new avenue for developing efficient and robust catalysts.

#### Conflicts of interest

There are no conflicts of interest to declare.

### Data availability

The data supporting this article have been included as part of the SI. Supplementary information is available. See DOI: https://doi.org/10.1039/d5dt02018b.

## Acknowledgements

This work is supported by Hebei North University 2025 College Students Innovation Training Program (no. 202510092022).

#### References

- 1 Y. Kohlhaas, Y. S. Tschauder, W. Plischka, U. Simon, R.-A. Eichel, M. Wessling and R. Keller, Joule, 2024, 8,
- 2 C. Mao, J. Byun, H. W. MacLeod, C. T. Maravelias and G. A. Ozin, Joule, 2024, 8, 1224-1238.
- 3 R. Ge, J. Huo, P. Lu, Y. Dou, Z. Bai, W. Li, H. Liu, B. Fei and S. Dou, Adv. Mater., 2024, 36, 2412031.
- 4 X. Peng, L. Zeng, D. Wang, Z. Liu, Y. Li, Z. Li, B. Yang, L. Lei, L. Dai and Y. Hou, Chem. Soc. Rev., 2023, 52, 2193-
- 5 J. Liu, S. Zhang, Y. Jiang, W. Li, M. Jin, J. Ding, Y. Zhang, G. Wang and H. Zhang, Chem. Commun., 2024, 60, 11592-
- 6 Y. Wu, H. Lin, Q. Mao, H. Yu, K. Deng, J. Wang, L. Wang, Z. Wang and H. Wang, Small, 2024, 20, 2407679.
- 7 S. Zhang, M. Jin, H. Xu, X. Zhang, T. Shi, Y. Ye, Y. Lin, L. Zheng, G. Wang, Y. Zhang, H. Yin, H. Zhang and H. Zhao, Energy Environ. Sci., 2024, 17, 1950-1960.
- 8 Z. Wang, Y. Wang, S. Xu, K. Deng, H. Yu, Y. Xu, H. Wang and L. Wang, J. Mater. Chem. A, 2025, 13, 305-311.
- 9 Y. Huang, R. Yang, C. Wang, N. Meng, Y. Shi, Y. Yu and B. Zhang, ACS Energy Lett., 2022, 7, 284-291.
- 10 D. Chen, J. Liu, J. Shen, Y. Zhang, H. Shao, C. Chen and S. Wang, Adv. Energy Mater., 2024, 14, 2303820.
- T. Hannagan, G. Giannakakis, Flytzani-11 R. Stephanopoulos and E. C. H. Sykes, Chem. Rev., 2020, 120, 12044-12088.
- 12 T. Zhang, A. G. Walsh, J. Yu and P. Zhang, Chem. Soc. Rev., 2021, 50, 569-588.
- 13 M. Xu, F. Wu, Y. Zhang, Y. Yao, G. Zhu, X. Li, L. Chen, G. Jia, X. Wu, Y. Huang, P. Gao and W. Ye, Nat. Commun., 2023, 14, 6994.

- 14 S. Zhang, J. Geng, Z. Zhao, M. Jin, W. Li, Y. Ye, K. Li, G. Wang, Y. Zhang, H. Yin, H. Zhang and H. Zhao, *EES Catal.*, 2023, 1, 45–53.
- 15 K. Chen, D. Ma, Y. Zhang, F. Wang, X. Yang, X. Wang, H. Zhang, X. Liu, R. Bao and K. Chu, Adv. Mater., 2024, 36, 2402160.
- 16 K. Chen, J. Xiang, Y. Guo, X. Liu, X. Li and K. Chu, *Nano Lett.*, 2024, 24, 541–548.
- 17 X. Li, P. Shen, X. Li, D. Ma and K. Chu, *ACS Nano*, 2023, **17**, 1081–1090.
- 18 P. Lu, X. Tan, H. Zhao, Q. Xiang, K. Liu, X. Zhao, X. Yin, X. Li, X. Hai and S. Xi, *ACS Nano*, 2021, **15**, 5671–5678.
- 19 W. Guo, X. Tan, J. Bi, L. Xu, D. Yang, C. Chen, Q. Zhu, J. Ma, A. Tayal and J. Ma, J. Am. Chem. Soc., 2021, 143, 6877–6885.
- 20 J. Li, M. Zhu and Y. F. Han, ChemCatChem, 2021, 13, 514-531
- 21 S. Li, X. Lu, S. Zhao, M. Ceccato, X.-M. Hu, A. Roldan, M. Liu and K. Daasbjerg, *ACS Catal.*, 2022, **12**, 7386–7395.
- 22 R. Lang, X. Du, Y. Huang, X. Jiang, Q. Zhang, Y. Guo, K. Liu, B. Qiao, A. Wang and T. Zhang, *Chem. Rev.*, 2020, 120, 11986–12043.
- 23 S. K. Kaiser, Z. Chen, D. Faust Akl, S. Mitchell and J. Pérez-Ramírez, *Chem. Rev.*, 2020, **120**, 11703–11809.
- 24 C. Gao, J. Low, R. Long, T. Kong, J. Zhu and Y. Xiong, *Chem. Rev.*, 2020, **120**, 12175–12216.
- 25 D. Wu, K. Chen, P. Lv, Z. Ma, K. Chu and D. Ma, *Nano Lett.*, 2024, 24, 8502–8509.

- 26 J. Min, J. Zhai, T. Dong, D. Xu, Y. Yan, C. S. Garoufalis, S. Baskoutas, Z. Zeng and Y. Jia, *Nano Lett.*, 2023, 23, 4648– 4653.
- 27 J. Zhai, T. Dong, Y. Zhou, J. Min, Y. Yan, C. S. Garoufalis, S. Baskoutas, D. Xu and Z. Zeng, *Nano Lett.*, 2023, 23, 3239–3244.
- 28 Z. Zhao, J. Zhang, M. Lei and Y. Lum, *Nano Res. Energy*, 2023, 2, e9120044.
- 29 W. Gou, H. Sun and F. Cheng, *Nano Res. Energy*, 2024, 3, e9120121.
- 30 Q. Wang, H. Wei, P. Liu, Z. Su and X.-Q. Gong, *Nano Res. Energy*, 2024, 3, e9120112.
- 31 Y. Cheng, H. Wang, H. Song, K. Zhang, G. I. Waterhouse, J. Chang, Z. Tang and S. Lu, *Nano Res. Energy*, 2023, 2, e9120082.
- 32 J. Shen and D. Wang, Nano Res. Energy, 2023, 3, e9120096.
- 33 Q. Hu, W. Zhou, S. Qi, Q. Huo, X. Li, M. Lv, X. Chen, C. Feng, J. Yu, X. Chai, H. Yang and C. He, *Nat. Sustain.*, 2024, 7, 442–451.
- 34 Y. Gao, J. Wang, M. Sun, Y. Jing, L. Chen, Z. Liang, Y. Yang, C. Zhang, J. Yao and X. Wang, *Angew. Chem., Int. Ed.*, 2024, 136, e202402215.
- 35 Y. Luo, K. Xie, P. Ou, C. Lavallais, T. Peng, Z. Chen, Z. Zhang, N. Wang, X.-Y. Li, I. Grigioni, B. Liu, D. Sinton, J. B. Dunn and E. H. Sargent, *Nat. Catal.*, 2023, 6, 939–948.
- 36 C. Lv, L. Zhong, H. Liu, Z. Fang, C. Yan, M. Chen, Y. Kong, C. Lee, D. Liu, S. Li, J. Liu, L. Song, G. Chen, Q. Yan and G. Yu, *Nat. Sustain.*, 2021, 4, 868–876.